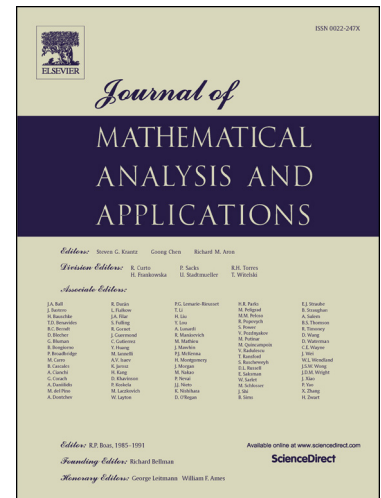


This is a PDF file of an unedited manuscript that has been accepted for publication. As a service to our customers we are providing this early version of the manuscript. The manuscript will undergo copyediting, typesetting, and review of the resulting proof before it is published in its final form. Please note that during the production process errors may be discovered which could affect the content, and all legal disclaimers that apply to the journal pertain.



Darboux transformation and rogue wave solutions for the variable-coefficients coupled Hirota equations

Xin Wang^a, Chong Liu^b, Lei Wang^c

^a*Department of Mathematics, Zhongyuan University of Technology, Zhengzhou, 450007, China*

^b*School of Physics, Northwest University, Xi'an, 710069, China*

^c*Department of Mathematics and Physics, North China Electric Power University, Beijing, 102206, China*

Abstract

We construct the Lax pair and Darboux transformation for the variable-coefficients coupled Hirota equations. Based on modulation instability and by taking the limit approach, we derive two types of N th-order rogue wave solutions with different dynamic structures in compact determinant representations. The explicit first-order rogue wave solution is presented, prolific vector rogue-wave patterns such as the dark-bright, composite, three-sister, quadruple and sextuple rogue waves with multiple compression points are demonstrated. In particular, in contrast to the standard Peregrine combs, unusual vector rogue wave combs such as the dark-bright and composite rogue wave combs are revealed by choosing sufficiently large periodic modulation amplitudes. Further, some wave characteristics such as the difference between light intensity and continuous wave background, and pulse energy evolution of the dark rogue wave solution that features multiple compression points are discussed in detail.

Keywords: Integrable system; Darboux transformation; rogue wave; variable-coefficients coupled Hirota equations.

1. Introduction

Originally termed to describe monstrous sea wave events in oceanography [1, 2], rogue waves have been at the center of considerable research activity to a great extent due to their emerging relevance in a great variety of realms. These includes, the nonlinear optics [3], Bose-Einstein condensates (BEC) [4], atmosphere [5], surface plasma [6], and even econophysics [7]. They suddenly emerge with an amplitude significantly larger than that of the surrounding wave crests and vanish without slighting trace, and can be generally expressed by rational polynomials in mathematics [8]. Nowadays, it is widely accepted that the modulation instability (MI) is the fundamental mechanism for the generation of the rogue waves [9].

The foremost description of a single rogue wave is the Peregrine solution [10], a rational solution of the nonlinear Schrödinger (NLS) equation which features a localized peak whose amplitude is three times larger than that of the average height. Subsequently, the more complicated rogue waves which can be represented by higher-order rational functions have been systematically investigated for the NLS equation [11–13]. Additionally, recent experiments in a water tank indicate that the actual dynamics of these extreme waves can be commendably described by the analytic solutions [14, 15].

*Corresponding author.

Email address: wangxinlinzhou@163.com (Xin Wang^a)

Considering the various physical contexts, one should go beyond the standard NLS representation to make further efforts to reveal the complex dynamics of rogue waves. Therefore, some important generalized higher-order systems (e.g. the Hirota equation [16], quartic NLS equations [17, 18] and Kundu-Eckhaus equation [19]) and coupled systems (e.g. the Manakov system [20–26], coupled Hirota equations [27–29] and three-wave resonant interaction equations [30]) have been paid widespread concern. In fact, it is confirmed that the higher-order dispersion and/or nonlinear terms play a pivotal pole in affecting the dynamics of rogue waves, including their ‘ridge’ [16] and temporal-spacial distributions [31], etc. Especially, the very recent reports on ‘breather-to-soliton’ and ‘transition’ properties show that the interesting W-shaped soliton can exist in the higher-order NLS equations instead of the standard NLS model without higher-order effects [32–34]. In addition, it is recognized that rogue waves in coupled systems can display diversity and complexity, which contains, the rogue wave-breather/soliton interactional structure [20, 29], dark structure [22], composite structure [24], four-petaled structure [35], and so forth.

Management of rogue waves in inhomogeneous nonlinear systems such as nonlinear fiber and BECs has also received extensive attention within the past decade [36–40]. A surge of work have been reported on involving controlling rogue waves in nonautonomous single or multi-components NLS equations with space and/or time modulated potentials like periodic potentials, harmonic potential, to name a few [36]. In particular, very recently, Tiofack et al. study the comb generation of the periodically modulated NLS equation by using the multiple compression points approach, which paves an important way for the experimental control and manipulation of nonautonomous rogue waves modeled by the NLS equation [41].

The propagation of vector optical rogue waves with higher-order effects in inhomogeneous optical fibers is described by the variable-coefficients coupled Hirota (VCCH) equations [42, 43], which can be written as the following dimensionless form:

$$iu_{1t} + \alpha(t)u_{1xx} + 2\delta(t)(|u_1|^2 + |u_2|^2)u_1 + i\beta(t)[u_{1xxx} + \gamma(t)(6|u_1|^2 + 3|u_2|^2)u_{1x} + 3\gamma(t)u_1u_2^*u_{2x}] + i\Gamma(t)u_1 = 0, \quad (1)$$

$$iu_{2t} + \alpha(t)u_{2xx} + 2\delta(t)(|u_1|^2 + |u_2|^2)u_2 + i\beta(t)[u_{2xxx} + \gamma(t)(6|u_2|^2 + 3|u_1|^2)u_{2x} + 3\gamma(t)u_2u_1^*u_{1x}] + i\Gamma(t)u_2 = 0, \quad (2)$$

where

$$\gamma(t) = \frac{\delta(t)}{\alpha(t)}, \quad \Gamma(t) = \frac{1}{2} \left[\frac{\delta(t)_t}{\delta(t)} - \frac{\alpha(t)_t}{\alpha(t)} \right]$$

is satisfied to ensure the Painlevé integrability of Eqs. (1)-(2). The potentials $u_1(x, t)$, $u_2(x, t)$ are the complex wave envelopes, t and x represent the propagation distance and transverse coordinate, and $*$ means complex conjugate. $\alpha(t)$, $\beta(t)$, $\delta(t)$, $\gamma(t)$ and $\Gamma(t)$ are restricted to periodic functions and stand for group velocity dispersion (GVD), third-order dispersion (TOD), nonlinear terms referred to self-phase modulation (SPM) and cross-phase modulation (XPM), nonlinear terms related to self-steepening (SS) and delayed nonlinear response, and gain or absorption modulus, respectively.

In the present work, we construct the Lax pair and Darboux transformation (DT) for Eqs. (1)-(2) by making use of the Ablowitz-Kaup-Newell-Segur (AKNS) technique [44]. Next based on the MI analysis [21, 45, 46] and by taking the limit approach [47–51], we derive two kinds of N th-order rogue wave solutions in compact determinant representations for Eqs. (1)-(2). The explicit first-order rogue wave solution is presented, and the dark-bright and composite rogue waves with multiple compression points are shown under the sinusoidally varying coefficients modulated conditions. Then the dark-bright and composite Peregrine combs are generated from the multiple compression points,

as long as the amplitude of the periodic modulation is sufficiently largely chosen. For the second-order circumstance, the dark-bright three sisters, rogue wave quartets and sextets structures containing one or more rogue waves with multiple compression points are displayed, respectively. The rest of this paper discuss some important wave characteristics such as the difference between light intensity and continuous-wave (CW) background, and pulse energy evolution to the dark rogue wave solution features multiple compression points.

The paper is structured as follows. In section 2, the Lax pair and N -fold DT are constructed. In section 3, the linear stability of a CW solution regarding to MI is analyzed. In section 4, two types of N th-order rogue wave solutions are derived. In section 5, rogue waves with multiple compression points are studied. In section 6, further properties of the dark rogue wave solution are discussed. Finally, we summarize our results and provide some discussions.

2. Lax pair and Darboux transformation

In this section, we first present the Lax pair of Eqs. (1)-(2) which can be constructed through the AKNS technique:

$$\Psi_x = U\Psi, \quad U = \zeta U_0 + U_1, \quad (3)$$

$$\Psi_t = V\Psi, \quad V = \zeta^3 V_0 + \zeta^2 V_1 + \zeta V_2 + V_3, \quad (4)$$

where

$$U_0 = \begin{pmatrix} -2i & 0 & 0 \\ 0 & i & 0 \\ 0 & 0 & i \end{pmatrix}, \quad U_1 = i\sqrt{\frac{\delta(t)}{\alpha(t)}} \begin{pmatrix} 0 & u_1 & u_2 \\ u_1^* & 0 & 0 \\ u_2^* & 0 & 0 \end{pmatrix}, \quad V_0 = 9i\beta(t)U_0, \quad V_1 = 3\alpha(t)U_0 + 9\beta(t)U_1,$$

$$V_2 = 3i\sqrt{\frac{\delta(t)}{\alpha(t)}} \begin{pmatrix} \sqrt{\frac{\delta(t)}{\alpha(t)}}\beta(t)(|u_1|^2 + |u_2|^2) & i\beta(t)u_{1x} + \alpha(t)u_1 & i\beta(t)u_{2x} + \alpha(t)u_2 \\ -i\beta(t)u_{1x}^* + \alpha(t)u_1^* & -\sqrt{\frac{\delta(t)}{\alpha(t)}}\beta(t)|u_1|^2 & -\sqrt{\frac{\delta(t)}{\alpha(t)}}\beta(t)u_1^*u_2 \\ -i\beta(t)u_{2x}^* + \alpha(t)u_2^* & -\sqrt{\frac{\delta(t)}{\alpha(t)}}\beta(t)u_1u_2^* & -\sqrt{\frac{\delta(t)}{\alpha(t)}}\beta(t)|u_2|^2 \end{pmatrix},$$

$$V_3 = \begin{pmatrix} \beta(t)(e_1 + e_2) + i\delta(t)(|u_1|^2 + |u_2|^2) & \beta(t)e_3 - \sqrt{\alpha(t)\delta(t)}u_{1x} & \beta(t)e_4 - \sqrt{\alpha(t)\delta(t)}u_{2x} \\ -\beta(t)e_3^* + \sqrt{\alpha(t)\delta(t)}u_{1x}^* & -\beta(t)e_1 - i\delta(t)|u_1|^2 & -\beta(t)e_5 - i\delta(t)u_1^*u_2 \\ -\beta(t)e_4^* + \sqrt{\alpha(t)\delta(t)}u_{2x}^* & \beta(t)e_5^* - i\delta(t)u_1u_2^* & -\beta(t)e_2 - i\delta(t)|u_2|^2 \end{pmatrix},$$

with

$$e_1 = -\frac{\delta(t)}{\alpha(t)} \left(u_1^* u_{1x} - u_1 u_{1x}^* \right), \quad e_2 = -\frac{\delta(t)}{\alpha(t)} \left(u_2^* u_{2x} - u_2 u_{2x}^* \right),$$

$$e_3 = -i\sqrt{\frac{\delta(t)}{\alpha(t)}} \left[u_{1xx} + 2\frac{\delta(t)}{\alpha(t)}(|u_1|^2 + |u_2|^2)u_1 \right],$$

$$e_4 = -i\sqrt{\frac{\delta(t)}{\alpha(t)}} \left[u_{2xx} + 2\frac{\delta(t)}{\alpha(t)}(|u_1|^2 + |u_2|^2)u_2 \right],$$

$$e_5 = -\frac{\delta(t)}{\alpha(t)} \left(u_1^* u_{2x} - u_2 u_{1x}^* \right).$$

The compatibility of the above Lax pair straightforwardly leads to Eqs. (1)-(2). On basis of the DT of the AKNS system [52], we can directly give the following lemma.

Lemma 1. *The standard DT*

$$\Psi[1] = T[1]\Psi, \quad T[1] = I - \frac{\Psi_1 \Psi_1^\dagger}{\zeta - \zeta_1^*} \left(\frac{\Psi_1^\dagger \Psi_1}{\zeta_1 - \zeta_1^*} \right)^{-1}, \quad (5)$$

here I is the unit matrix, and \dagger represents Hermite conjugation, converts the linear spectral problem (3)-(4) into a new system with the same form, that is

$$\begin{aligned} \Psi[1]_x &= U[1](\zeta, u_i[1])\Psi[1], \\ \Psi[1]_t &= V[1](\zeta, u_i[1])\Psi[1], \end{aligned}$$

where $\Psi_1 = (\psi_1, \phi_1, \chi_1)^T$ is a basic solution of the linear spectral problem (3)-(4) at $\zeta = \zeta_1$ and the initial solution of $u_i = u_i[0]$ ($i = 1, 2$), and

$$u_1[1] = u_1[0] + 3\sqrt{\frac{\alpha(t)}{\delta(t)}} \frac{(\zeta_1^* - \zeta_1)}{\Psi_1^\dagger \Psi_1} \psi_1 \phi_1^*, \quad (6a)$$

$$u_2[1] = u_2[0] + 3\sqrt{\frac{\alpha(t)}{\delta(t)}} \frac{(\zeta_1^* - \zeta_1)}{\Psi_1^\dagger \Psi_1} \psi_1 \chi_1^*. \quad (6b)$$

Afterwards, assume we have N distinct basic solutions $\Psi_i = (\psi_i, \phi_i, \chi_i)^T$ of Eqs. (3)-(4) at $\zeta = \zeta_i$ and $u_i = u_i[0]$. According to the higher-degree Darboux matrix theorem [52], we can end up with the general form of the standard DT.

Lemma 2. *The N -fold DT takes the form*

$$T_N = I - X M^{-1} (\zeta - J)^{-1} X^\dagger, \quad (7)$$

$$u_1[N] = u_1[0] + 3\sqrt{\frac{\alpha(t)}{\delta(t)}} \frac{\det(M_1)}{\det(M)}, \quad (8)$$

$$u_2[N] = u_2[0] + 3\sqrt{\frac{\alpha(t)}{\delta(t)}} \frac{\det(M_2)}{\det(M)}, \quad (9)$$

where

$$\begin{aligned} X &= (\Psi_1, \Psi_2, \dots, \Psi_N), \quad J = \text{diag}\{\zeta_1^*, \zeta_2^*, \dots, \zeta_N^*\}, \\ M_1 &= \begin{pmatrix} \frac{\Psi_1^\dagger \Psi_1}{\zeta_1 - \zeta_1^*} & \frac{\Psi_2^\dagger \Psi_1}{\zeta_1 - \zeta_2^*} & \dots & \frac{\Psi_N^\dagger \Psi_1}{\zeta_1 - \zeta_N^*} & \phi_1^* \\ \frac{\Psi_1^\dagger \Psi_2}{\zeta_2 - \zeta_1^*} & \frac{\Psi_2^\dagger \Psi_2}{\zeta_2 - \zeta_2^*} & \dots & \frac{\Psi_N^\dagger \Psi_2}{\zeta_2 - \zeta_N^*} & \phi_2^* \\ \vdots & \vdots & \ddots & \vdots & \vdots \\ \frac{\Psi_1^\dagger \Psi_N}{\zeta_N - \zeta_1^*} & \frac{\Psi_2^\dagger \Psi_N}{\zeta_N - \zeta_2^*} & \dots & \frac{\Psi_N^\dagger \Psi_N}{\zeta_N - \zeta_N^*} & \phi_N^* \\ \psi_1 & \psi_2 & \dots & \psi_N & 0 \end{pmatrix}, \end{aligned}$$

$$M_2 = \begin{pmatrix} \frac{\Psi_1^\dagger \Psi_1}{\zeta_1 - \zeta_1^*} & \frac{\Psi_2^\dagger \Psi_1}{\zeta_1 - \zeta_2^*} & \cdots & \frac{\Psi_N^\dagger \Psi_1}{\zeta_1 - \zeta_N^*} & \chi_1^* \\ \frac{\Psi_1^\dagger \Psi_2}{\zeta_2 - \zeta_1^*} & \frac{\Psi_2^\dagger \Psi_2}{\zeta_2 - \zeta_2^*} & \cdots & \frac{\Psi_N^\dagger \Psi_2}{\zeta_2 - \zeta_N^*} & \chi_2^* \\ \vdots & \vdots & \ddots & \vdots & \vdots \\ \frac{\Psi_1^\dagger \Psi_N}{\zeta_N - \zeta_1^*} & \frac{\Psi_2^\dagger \Psi_N}{\zeta_N - \zeta_2^*} & \cdots & \frac{\Psi_N^\dagger \Psi_N}{\zeta_N - \zeta_N^*} & \chi_N^* \\ \psi_1 & \psi_2 & \cdots & \psi_N & 0 \end{pmatrix},$$

$$M = \begin{pmatrix} \frac{\Psi_1^\dagger \Psi_1}{\zeta_1 - \zeta_1^*} & \frac{\Psi_2^\dagger \Psi_1}{\zeta_1 - \zeta_2^*} & \cdots & \frac{\Psi_N^\dagger \Psi_1}{\zeta_1 - \zeta_N^*} \\ \frac{\Psi_1^\dagger \Psi_2}{\zeta_2 - \zeta_1^*} & \frac{\Psi_2^\dagger \Psi_2}{\zeta_2 - \zeta_2^*} & \cdots & \frac{\Psi_N^\dagger \Psi_2}{\zeta_2 - \zeta_N^*} \\ \vdots & \vdots & \ddots & \vdots \\ \frac{\Psi_1^\dagger \Psi_N}{\zeta_N - \zeta_1^*} & \frac{\Psi_2^\dagger \Psi_N}{\zeta_N - \zeta_2^*} & \cdots & \frac{\Psi_N^\dagger \Psi_N}{\zeta_N - \zeta_N^*} \end{pmatrix}.$$

Proof. By using the iterative rule of the one-fold DT, we have

$$T_N = T[N]T[N-1] \cdots T[1] = I + \sum_{i=1}^N \frac{C_i}{\zeta - \zeta_i^*}, \quad C_i = |x_i\rangle\langle y_i|,$$

where $|x_i\rangle$ is an undetermined column vector, and $\langle y_i| = \Psi_i^\dagger$ is a row vector. By taking into account of $T_N|_{\zeta=\zeta_i} \Psi_i = 0$, we obtain

$$(|x_1\rangle, |x_2\rangle, \dots, |x_N\rangle) = -(\Psi_1, \Psi_2, \dots, \Psi_N)M^{-1}, \quad M_{ij} = \frac{\Psi_i^* \Psi_j}{\zeta_j - \zeta_i^*}, \quad 1 \leq i, j \leq N.$$

This gives rise to Eq. (7) directly. Then inserting the expression of T_N into

$$T_{Nx} + T_N U = U[N]T_N,$$

holds

$$\sum_{i=1}^N \frac{C_{ix}}{\zeta - \zeta_i} + \left(I + \sum_{i=1}^N \frac{C_i}{\zeta - \zeta_i^*} \right) (\zeta U_0 + U_1) = (\zeta U_0 + U_1[N]) \left(I + \sum_{i=1}^N \frac{C_i}{\zeta - \zeta_i^*} \right).$$

By letting $\zeta \rightarrow \infty$, we arrive at

$$U_1[N] = U_1 + \sum_{i=1}^N [C_i, U_0],$$

where the commutator $[A, B] = AB - BA$. Then it follows that

$$u_1[N] = u_1[0] + 3\sqrt{\frac{\alpha(t)}{\delta(t)}} \sum_{i=1}^N (C_i)_{12} = \text{the rhs of (8)},$$

$$u_2[N] = u_2[0] + 3\sqrt{\frac{\alpha(t)}{\delta(t)}} \sum_{i=1}^N (C_i)_{13} = \text{the rhs of (9)}.$$

This completes the proof.

3. MI analysis

To study the interesting properties of rogue waves in Eqs. (1)-(2), we pay our attention to the standard MI analysis since MI is believed to be a fundamental mechanism for the formation of rogue waves [9]. In particular, the exact relation between rogue waves and the zero-frequency MI subregion has been established in several nonlinear systems [21, 45, 46]. Hence the MI characteristics will play a crucial role to study the rogue-wave properties in many different nonlinear wave systems.

Our starting point is a CW solution of Eqs. (1)-(2) with the generalized form

$$u_1[0] = \sqrt{\frac{\alpha(t)}{\delta(t)}} c_1 e^{i\theta_1}, \quad u_2[0] = \sqrt{\frac{\alpha(t)}{\delta(t)}} c_2 e^{i\theta_2}, \quad (10)$$

where $\theta_i = a_i x + b_i(t)$ ($i = 1, 2$), c_i and a_i are real constants, which delegate the amplitudes and frequencies of the two CW backgrounds, respectively. Here, $b_i(t)$ will be determined in the following.

Note that the background amplitude difference between two CW modes have no substantive effects on the structure characteristics of the vector rogue waves. Thus we set $c_1 = c_2 = c$ without loss of generality. However, the background frequency difference plays a key role in the MI and localized wave dynamics since it cannot be omitted by the Galilean transformation. Indeed, it has been recently proved that the frequency relationship $a_1 - a_2 = 2a$ could bring about abundant types of rogue waves in coupled systems which has no analogue in scalar NLS model (see [24, 27, 34] and the references therein). It should be pointed out that if $a_1 = a_2$, the MI corresponds to the trivial vector generalization of scalar Hirota MI [33].

Accordingly, we now uniformly set the CW fields with equal amplitudes (i.e. $c_1 = c_2 = c$) and different frequencies (i.e. $a_1 = -a_2 = a$). At this point, the function $b_i(t)$ can be determined by

$$\begin{aligned} b_1(t) &= (4c^2 - a^2)A(t) + (a^3 - 6ac^2)B(t), \\ b_2(t) &= (4c^2 - a^2)A(t) - (a^3 - 6ac^2)B(t), \end{aligned}$$

where

$$A(t) = \int^t \alpha(t') dt' + A_0, \quad B(t) = \int^t \beta(t') dt' + B_0,$$

with A_0, B_0 being two integration constants.

Next we impose a small perturbation on the CW solution by taking

$$u_1 = u_1[0](1 + q_1), \quad u_2 = u_2[0](1 + q_2). \quad (11)$$

Substituting Eq. (11) into Eqs. (1)-(2) one can get the linearized VCCH equations as

$$\begin{aligned} i q_{1t} + (2\alpha c^2 - 6\beta a c^2)(q_1 + q_1^*) + 2\alpha c^2(q_2 + q_2^*) + i(9\beta c^2 - 3\beta a^2 + 2\alpha a)q_{1x} + 3i\beta c^2 q_{2x} \\ + (\alpha - 3\beta a)q_{1xx} + i\beta q_{1xxx} = 0, \end{aligned} \quad (12)$$

$$\begin{aligned} i q_{2t} + (2\alpha c^2 + 6\beta a c^2)(q_2 + q_2^*) + 2\alpha c^2(q_1 + q_1^*) + i(9\beta c^2 - 3\beta a^2 - 2\alpha a)q_{2x} + 3i\beta c^2 q_{1x} \\ + (\alpha + 3\beta a)q_{2xx} + i\beta q_{2xxx} = 0. \end{aligned} \quad (13)$$

The stability of the solution of the above linearized equations to wavelength κ can be studied by

collecting the Fourier modes in the following way:

$$q_1 = f_+ \exp[i\kappa(x - \Omega(t))] + f_-^* \exp[-i\kappa(x - \Omega(t)^*)], \quad q_2 = g_+ \exp[i\kappa(x - \Omega(t))] + g_-^* \exp[-i\kappa(x - \Omega(t)^*)], \quad (14)$$

where $\Omega(t)$ is a non-real function corresponding to instability. Putting Eq. (14) into Eqs. (12)-(13) and to ensure the equations about $\{f_+, f_-, g_+, g_-\}$ be solvable we have

$$\begin{aligned} \Omega(t) = & (9c^2 - 3a^2 - \kappa^2)B(t) + 3\sqrt{c^4 - 4a^2c^2 + \kappa^2a^2}B(t) \\ & + \sqrt{4a^2 - 4c^2 + \kappa^2 - 4\sqrt{c^4 - 4a^2c^2 + \kappa^2a^2}}A(t). \end{aligned}$$

Afterwards, the marginal stability curves which are related to the higher-order effects $B(t)$ (i.e. TOD, SS and SRS) are given by

$$\kappa = \pm \frac{c}{a} \sqrt{4a^2 - c^2}.$$

When $0 < c^2 < 4a^2$, the MI growth rate can be influenced by the higher-order effects, and it has the form

$$\begin{aligned} \text{Im}\{\Omega(t)\} = & 3\sqrt{-c^4 + 4a^2c^2 - \kappa^2a^2}B(t) \\ & + \frac{1}{2}\sqrt{-2\kappa^2 - 8a^2 + 8c^2 + 2\sqrt{(4a^2 - \kappa^2)(4a^2 + 8c^2 - \kappa^2)}}A(t), \end{aligned} \quad (15)$$

such that the following stability condition is fulfilled,

$$\kappa^2 < \frac{c^2}{a^2}(4a^2 - c^2).$$

When $c^2 \geq 4a^2$, the higher-order effects do not influence the MI growth rate, which can be defined by

$$\text{Im}\{\Omega(t)\} = \sqrt{4c^2 - 4a^2 - \kappa^2 + 4\sqrt{c^4 - 4a^2c^2 + \kappa^2a^2}}A(t), \quad (16)$$

under the instability condition

$$4a^2 < \kappa^2 < 4a^2 + 8c^2.$$

The above two types of existences of MI actually provide the evidence of occurrence of rogue waves in Eqs. (1)-(2). In the next section, we will work out two types of N th-order rogue wave solutions based on the N -fold DT and MI.

4. N th-order rogue wave solutions

In the following, we substitute the general CW solution (10) into Eqs. (3)-(4), then the basic solution reads

$$\Psi = D \begin{pmatrix} \frac{1}{c} & \frac{1}{c} & \frac{1}{c} \\ \frac{1}{\xi_1 - \zeta - a} & \frac{1}{\xi_2 - \zeta - a} & \frac{1}{\xi_3 - \zeta - a} \\ \frac{1}{\xi_1 - \zeta + a} & \frac{1}{\xi_2 - \zeta + a} & \frac{1}{\xi_3 - \zeta + a} \end{pmatrix} \begin{pmatrix} \gamma_1 e^{iA_1} \\ \gamma_2 e^{iA_2} \\ \gamma_3 e^{iA_3} \end{pmatrix}, \quad (17)$$

where

$$\begin{aligned} D = & \text{diag}\{1, e^{-i\theta_1}, e^{-i\theta_2}\}, \\ A_i = & \xi_i x - [A(t) + 3\zeta B(t)]\xi_i^2 + [2\zeta A(t) + (a^2 - 4c^2 + 6\zeta^2)B(t)]\xi_i + (4c^2 + 2\zeta^2)A(t) \\ & + (4c^2\zeta + 2a^2\zeta + 6\zeta^3)B(t), \quad i = 1, 2, 3, \end{aligned} \quad (18)$$

with γ_i being arbitrary real constants, and ξ_i satisfying a cubic algebraic equation as

$$\xi^3 - (2c^2 + a^2 + 3\zeta^2)\xi + 2c^2\zeta - 2a^2\zeta + 2\zeta^3 = 0. \quad (19)$$

4.1. The case of $0 < c^2 < 4a^2$.

In this circumstance, it is found that the cubic algebraic equation (19) does not have a triple root. Nevertheless, by choosing adequate spectral parameter, one can prove that there exists a complex double root for the algebraic equation.

Without loss of generality, we set $a = 1, c = 1$, and choose the spectral parameter as

$$\zeta = \frac{z_1}{6} - \frac{\sqrt{3}}{2} \frac{i}{z_1} + \left[-\frac{z_1}{12} + i \left(\frac{z_1}{6} + \frac{\sqrt{3}}{12} z_1 \right) \right] \epsilon^2, \quad (20)$$

where $z_1 = \sqrt{6\sqrt{3} - 9}$, and ϵ is a complex small perturbation parameter. Then, we denote

$$\Phi_1 = \begin{pmatrix} \frac{1}{\xi_1 - \zeta - 1} & \frac{1}{\xi_2 - \zeta - 1} \\ \frac{1}{\xi_1 - \zeta + 1} & \frac{1}{\xi_2 - \zeta + 1} \end{pmatrix} \begin{pmatrix} e^{iA_1} \\ e^{iA_2} \end{pmatrix},$$

$$\Phi_2 = \begin{pmatrix} \frac{1}{\xi_1 - \zeta - 1} & \frac{1}{\xi_2 - \zeta - 1} \\ \frac{1}{\xi_1 - \zeta + 1} & \frac{1}{\xi_2 - \zeta + 1} \end{pmatrix} \begin{pmatrix} \frac{e^{iA_1}}{\epsilon} \\ -\frac{e^{iA_2}}{\epsilon} \end{pmatrix},$$

and

$$\Psi_1 = (\psi_1, \phi_1, \chi_1)^T = m\Phi_1 + n\Phi_2. \quad (21)$$

Here A_i, ξ_i ($i = 1, 2$) are determined by Eqs. (18)-(19) with $a = 1, c = 1$, ζ is fixed at (20), and

$$m = m_0 + m_1\epsilon^2 + \cdots + m_{N-1}\epsilon^{2(N-1)},$$

$$n = n_0 + n_1\epsilon^2 + \cdots + n_{N-1}\epsilon^{2(N-1)},$$

with m_j, n_j ($0 \leq j \leq N-1$) being arbitrary real constants. By making use of the limit approach of the N -fold DT, we can directly give the following theorem.

Theorem 1. The N th-order rogue wave solution for Eqs. (1)-(2) in the case of $0 < c^2 < 4a^2$ (more precisely, $a = 1, c = 1$) has the form

$$u_1[N] = \sqrt{\frac{\alpha(t)}{\delta(t)}} e^{i\theta_1} \frac{\det(P_1)}{\det(P)}, \quad (22a)$$

$$u_2[N] = \sqrt{\frac{\alpha(t)}{\delta(t)}} e^{i\theta_2} \frac{\det(P_2)}{\det(P)}, \quad (22b)$$

where

$$\theta_1 = x + 3A(t) - 5B(t), \quad \theta_2 = -x + 3A(t) + 5B(t),$$

$$\begin{aligned}
 P_1 &= P - 3 \begin{pmatrix} \phi_1^{[0]*} \psi_1^{[0]} & \phi_1^{[0]*} \psi_1^{[1]} & \cdots & \phi_1^{[0]*} \psi_1^{[N-1]} \\ \phi_1^{[1]*} \psi_1^{[0]} & \phi_1^{[1]*} \psi_1^{[1]} & \cdots & \phi_1^{[1]*} \psi_1^{[N-1]} \\ \vdots & \vdots & \ddots & \vdots \\ \phi_1^{[N-1]*} \psi_1^{[0]} & \phi_1^{[N-1]*} \psi_1^{[1]} & \cdots & \phi_1^{[N-1]*} \psi_1^{[N-1]} \end{pmatrix}, \\
 P_2 &= P - 3 \begin{pmatrix} \chi_1^{[0]*} \psi_1^{[0]} & \chi_1^{[0]*} \psi_1^{[1]} & \cdots & \chi_1^{[0]*} \psi_1^{[N-1]} \\ \chi_1^{[1]*} \psi_1^{[0]} & \chi_1^{[1]*} \psi_1^{[1]} & \cdots & \chi_1^{[1]*} \psi_1^{[N-1]} \\ \vdots & \vdots & \ddots & \vdots \\ \chi_1^{[N-1]*} \psi_1^{[0]} & \chi_1^{[N-1]*} \psi_1^{[1]} & \cdots & \chi_1^{[N-1]*} \psi_1^{[N-1]} \end{pmatrix}, \\
 P &= \begin{pmatrix} P[1, 1] & P[1, 2] & \cdots & P[1, N] \\ P[2, 1] & P[2, 2] & \cdots & P[2, N] \\ \vdots & \vdots & \ddots & \vdots \\ P[N, 1] & P[N, 2] & \cdots & P[N, N] \end{pmatrix},
 \end{aligned}$$

with

$$\begin{aligned}
 P[i, j] &= \frac{1}{2(i-1)!2(j-1)!} \frac{\partial^{2(i+j-2)}}{\partial \epsilon^{2(j-1)} \partial \epsilon^{*2(i-1)}} \frac{(|\psi_1|^2 + |\phi_1|^2 + |\chi_1|^2)}{\Delta_1} \Big|_{\epsilon, \epsilon^* \rightarrow 0}, \\
 \Delta_1 &= -i \frac{\sqrt{3}}{z_1} - \frac{z_1}{12} (\epsilon^2 - \epsilon^{*2}) + i \left(\frac{z_1}{6} + \frac{\sqrt{3}}{12} z_1 \right) (\epsilon^2 + \epsilon^{*2}), \\
 \psi_1^{[l]} &= \frac{1}{2l!} \frac{\partial^{2l} \psi_1}{\partial \epsilon^{2l}} \Big|_{\epsilon \rightarrow 0}, \quad \phi_1^{[l]} = \frac{1}{2l!} \frac{\partial^{2l} \phi_1}{\partial \epsilon^{2l}} \Big|_{\epsilon \rightarrow 0}, \quad \chi_1^{[l]} = \frac{1}{2l!} \frac{\partial^{2l} \chi_1}{\partial \epsilon^{2l}} \Big|_{\epsilon \rightarrow 0}.
 \end{aligned}$$

4.2. The case of $c^2 \geq 4a^2$.

In this situation, we focus on the case of $c^2 = 4a^2$, since it is readily to verify that the cubic algebraic equation (19) could possess a triple root at this point.

As before, for concreteness, we set $a = \frac{1}{2}$, $c = 1$ and choose the spectral parameter be

$$\zeta = \frac{\sqrt{3}}{2} i + \frac{\epsilon^3}{3}, \tag{23}$$

where ϵ is a complex small perturbation parameter as is mentioned before. Afterwards, we introduce

$$\begin{aligned}
 \Phi_1 &= \begin{pmatrix} 1 & 1 & 1 \\ \frac{1}{\xi_1 - \zeta - \frac{1}{2}} & \frac{1}{\xi_2 - \zeta - \frac{1}{2}} & \frac{1}{\xi_3 - \zeta - \frac{1}{2}} \\ 1 & 1 & 1 \\ \frac{1}{\xi_1 - \zeta + \frac{1}{2}} & \frac{1}{\xi_2 - \zeta + \frac{1}{2}} & \frac{1}{\xi_3 - \zeta + \frac{1}{2}} \end{pmatrix} \begin{pmatrix} e^{iA_1} \\ e^{iA_2} \\ e^{iA_3} \end{pmatrix}, \\
 \Phi_2 &= \begin{pmatrix} 1 & 1 & 1 \\ \frac{1}{\xi_1 - \zeta - \frac{1}{2}} & \frac{1}{\xi_2 - \zeta - \frac{1}{2}} & \frac{1}{\xi_3 - \zeta - \frac{1}{2}} \\ 1 & 1 & 1 \\ \frac{1}{\xi_1 - \zeta + \frac{1}{2}} & \frac{1}{\xi_2 - \zeta + \frac{1}{2}} & \frac{1}{\xi_3 - \zeta + \frac{1}{2}} \end{pmatrix} \begin{pmatrix} \frac{e^{iA_1}}{\epsilon} \\ \omega^* \frac{e^{iA_2}}{\epsilon} \\ \frac{e^{iA_3}}{\omega \epsilon} \end{pmatrix},
 \end{aligned}$$

$$\Phi_3 = \begin{pmatrix} \frac{1}{\xi_1 - \zeta - \frac{1}{2}} & \frac{1}{\xi_2 - \zeta - \frac{1}{2}} & \frac{1}{\xi_3 - \zeta - \frac{1}{2}} \\ \frac{1}{\xi_1 - \zeta + \frac{1}{2}} & \frac{1}{\xi_2 - \zeta + \frac{1}{2}} & \frac{1}{\xi_3 - \zeta + \frac{1}{2}} \end{pmatrix} \begin{pmatrix} \frac{e^{iA_1}}{\epsilon^2} \\ \frac{e^{iA_2}}{\omega \epsilon^2} \\ \frac{e^{iA_3}}{\omega^* \epsilon^2} \end{pmatrix},$$

and

$$\Psi_1 = (\psi_1, \phi_1, \chi_1)^T = m\Phi_1 + n\Phi_2 + s\Phi_3. \quad (24)$$

Here $\omega = e^{2\pi i/3}$, A_i , ξ_i ($i = 1, 2, 3$) are determined by Eqs. (18)-(19) with $a = \frac{1}{2}$, $c = 1$, ζ is chosen as (23), and

$$\begin{aligned} m &= m_0 + m_1\epsilon^3 + \cdots + m_{N-1}\epsilon^{3(N-1)}, \\ n &= n_0 + n_1\epsilon^3 + \cdots + n_{N-1}\epsilon^{3(N-1)}, \\ s &= s_0 + s_1\epsilon^3 + \cdots + s_{N-1}\epsilon^{3(N-1)}, \end{aligned}$$

with m_j , n_j and s_j ($0 \leq j \leq N-1$) being arbitrary real constants. Similarly, by using the limit approach of the N -fold DT, we immediately have the following theorem.

Theorem 2. *The N th-order rogue wave solution for Eqs. (1)-(2) in the case of $c^2 \geq 4a^2$ (or rather, $a = \frac{1}{2}$, $c = 1$) takes the form*

$$u_1[N] = \sqrt{\frac{\alpha(t)}{\delta(t)}} e^{i\theta_1} \frac{\det(Q_1)}{\det(Q)}, \quad (25a)$$

$$u_2[N] = \sqrt{\frac{\alpha(t)}{\delta(t)}} e^{i\theta_2} \frac{\det(Q_2)}{\det(Q)}, \quad (25b)$$

where

$$\begin{aligned} \theta_1 &= \frac{1}{2}x + \frac{15}{4}A(t) - \frac{23}{8}B(t), \quad \theta_2 = -\frac{1}{2}x + \frac{15}{4}A(t) + \frac{23}{8}B(t), \\ Q_1 &= Q - 3 \begin{pmatrix} \phi_1^{[0]*} \psi_1^{[0]} & \phi_1^{[0]*} \psi_1^{[1]} & \cdots & \phi_1^{[0]*} \psi_1^{[N-1]} \\ \phi_1^{[1]*} \psi_1^{[0]} & \phi_1^{[1]*} \psi_1^{[1]} & \cdots & \phi_1^{[1]*} \psi_1^{[N-1]} \\ \vdots & \vdots & \ddots & \vdots \\ \phi_1^{[N-1]*} \psi_1^{[0]} & \phi_1^{[N-1]*} \psi_1^{[1]} & \cdots & \phi_1^{[N-1]*} \psi_1^{[N-1]} \end{pmatrix}, \\ Q_2 &= Q - 3 \begin{pmatrix} \chi_1^{[0]*} \psi_1^{[0]} & \chi_1^{[0]*} \psi_1^{[1]} & \cdots & \chi_1^{[0]*} \psi_1^{[N-1]} \\ \chi_1^{[1]*} \psi_1^{[0]} & \chi_1^{[1]*} \psi_1^{[1]} & \cdots & \chi_1^{[1]*} \psi_1^{[N-1]} \\ \vdots & \vdots & \ddots & \vdots \\ \chi_1^{[N-1]*} \psi_1^{[0]} & \chi_1^{[N-1]*} \psi_1^{[1]} & \cdots & \chi_1^{[N-1]*} \psi_1^{[N-1]} \end{pmatrix}, \\ Q &= \begin{pmatrix} Q[1, 1] & Q[1, 2] & \cdots & Q[1, N] \\ Q[2, 1] & Q[2, 2] & \cdots & Q[2, N] \\ \vdots & \vdots & \ddots & \vdots \\ Q[N, 1] & Q[N, 2] & \cdots & Q[N, N] \end{pmatrix}, \end{aligned}$$

with

$$Q[i, j] = \frac{1}{3(i-1)!3(j-1)!} \frac{\partial^{3(i+j-2)}}{\partial \epsilon^{3(j-1)} \partial \epsilon^{*3(i-1)}} \frac{(|\psi_1|^2 + |\phi_1|^2 + |\chi_1|^2)}{\Delta_2} \Big|_{\epsilon \rightarrow 0, \epsilon^* \rightarrow 0},$$

$$\Delta_2 = \sqrt{3}i + \frac{\epsilon^3}{3} - \frac{\epsilon^{*3}}{3}, \quad \psi_1^{[l]} = \frac{1}{3!} \frac{\partial^{3l} \psi_1}{\partial \epsilon^{3l}} \Big|_{\epsilon \rightarrow 0}, \quad \phi_1^{[l]} = \frac{1}{3!} \frac{\partial^{3l} \phi_1}{\partial \epsilon^{3l}} \Big|_{\epsilon \rightarrow 0}, \quad \chi_1^{[l]} = \frac{1}{3!} \frac{\partial^{3l} \chi_1}{\partial \epsilon^{3l}} \Big|_{\epsilon \rightarrow 0}.$$

5. Rogue waves with multiple compression points

This section is devoted to study dynamics of the dark-bright and composite rogue waves with multiple compression points.

5.1. Dark-bright rogue waves

By resorting to Eqs. (22a)-(22b) for $N = 1$, one can obtain the rogue wave solution with the form

$$u_1[1] = \sqrt{\frac{\alpha(t)}{\delta(t)}} e^{i\theta_1} \frac{\rho_1(G_1 + iH_1)}{F}, \quad (26a)$$

$$u_2[1] = \sqrt{\frac{\alpha(t)}{\delta(t)}} e^{i\theta_2} \frac{\rho_2(G_2 + iH_2)}{F}, \quad (26b)$$

where the corresponding polynomials and constants are given in appendix, and we have set $\beta(t) = \nu\alpha(t)$ with ν being a small real constant and $m_0 = 5$, $m_1 = 0$.

To proceed, as is discussed in [36, 41], we suppose the GVD-TOD periodic modulation functions follow the form

$$\alpha(t) = \beta(t)/\nu = 1 - d \cos(kt), \quad (27)$$

and the SPM-XPM periodic modulation function be determined by the equation

$$\sqrt{\frac{\alpha(t)}{\delta(t)}} = 1 - \tilde{d} \sin(\tilde{k}t), \quad (28)$$

where d, \tilde{d} are the amplitudes of modulations, and k, \tilde{k} represent the frequencies. At this point, we get

$$A(t) = t - \frac{d}{k} \sin(kt) + A_0.$$

After that, we discuss the rogue wave dynamics described by Eqs. (26a)-(26b). As a matter of fact, it is readily to find that rogue wave solution in this case features the dark-bright structure, and one can also compute that the minimum and maximum values of the wave amplitudes in u_1 and u_2 components occur at $(x, A(t)) = (2.11, -2.10)$. Hence, when putting $A_0 = -2.10$, the number of the compression points for the rogue wave can be determined by the number of the solutions to the following equation

$$t - \frac{d}{k} \sin(kt) = 0. \quad (29)$$

It is known that the explicit closed form expression for the solutions of the above transcendental equation is not available. Whereas it is can be checked that as the value of d increases, the number

of the solutions increases in pairs. To be specific, by using the compression points analysis [41], we denote

$$d_\ell = \frac{\pi}{2} + 2\ell\pi, \quad \ell \geq 1,$$

then it is calculated that when d increases from d_ℓ to $d_{\ell+1}$, the new solutions of Eq. (29) are generated and can be approximately localized at

$$t = \pm \frac{d_\ell}{k}.$$

Taking into account of the above facts, we can provide an exact calculation formula for the number of the compression points, which is closely related to the value of the amplitude of modulation. We define it as $N_{cp}(d)$, then it holds that

$$N_{cp}(d) = \begin{cases} 1, & d \in [0, 1], \\ 3, & d \in (1, d_1), \\ 4\ell + 1, & d = d_\ell, \ell \geq 1, \\ 4\ell + 3, & d \in (d_\ell, d_{\ell+1}), \ell \geq 1. \end{cases} \quad (30)$$

In what follows, on basis of the formula (30), we present some concrete examples to illustrate the management of the nonautonomous rogue waves with multiple compression points.

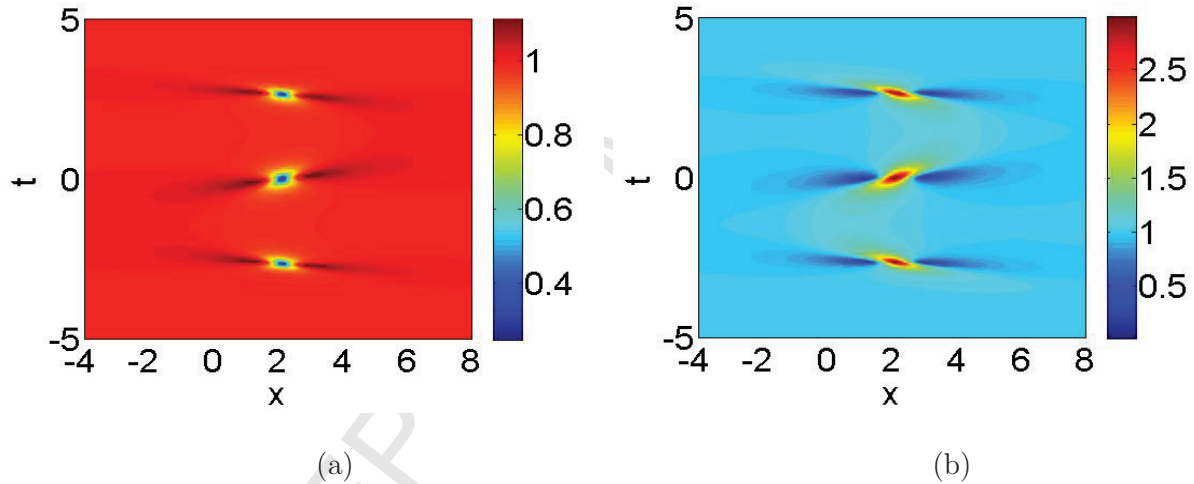


Fig. 1: Intensity of the solution (26a)-(26b) with $d = 3\pi/4, k = \pi/4, \tilde{d} = 0, A_0 = -2.10$ and $\nu = 0.1$. (a), (b) Dark-bright rogue waves with triple compression points in u_1 and u_2 components.

We first choose $d = 3\pi/4 \in (1, d_1)$, then it is apparent to see that in Fig. 1, there exist triple compression points for the dark-bright rogue waves, which can not be found in the constant-coefficient systems. While when taking $d \rightarrow 0$ and $\tilde{d} \rightarrow 0$, the rogue wave solution (26a)-(26b) is reduced into the standard Peregrine soliton. The corresponding shape comparison between the standard Peregrine rogue wave and the rogue wave with triple compression points is displayed in Fig. 2. At this point, it is expressly to observe that the single compression point split in two when d from 0 to $3\pi/4$. Moreover, as the value of d is sufficiently large, for instance, by changing $d = 15\pi/4 \in (d_1, d_2)$, then the dark-bright comb-like structures can be generated, see Fig. 3. Hereby, it is clearly seen that the dark-bright rogue waves with sevenfold ($4 \times 1 + 3 = 7$) compression points come into being with a comb-like structure. In addition, it is naturally to note that the frequency constant k only controls the distance among each multiple compression points, but it does not affect the main rogue wave characteristics.

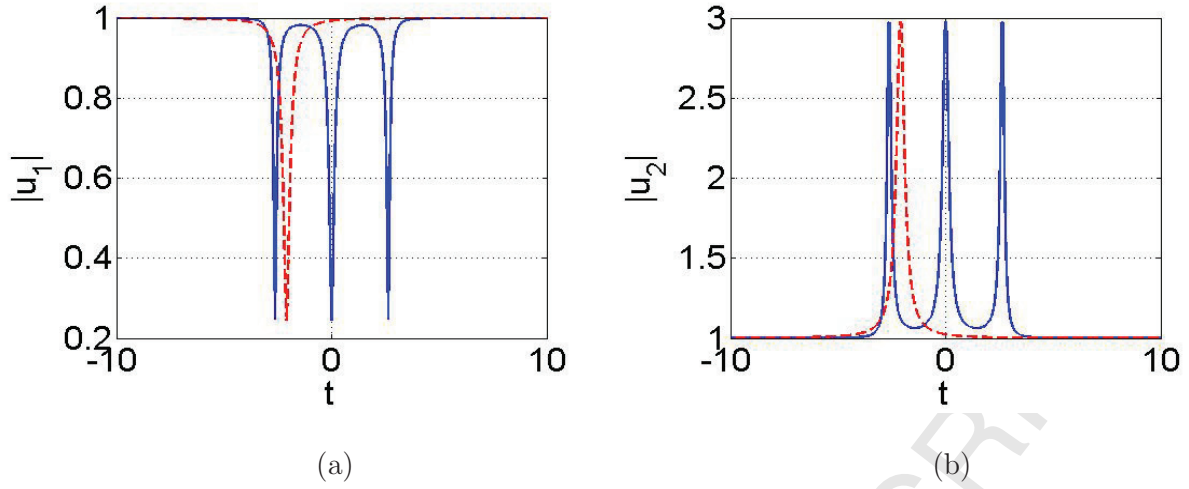


Fig. 2: Shape of the solution (26a)-(26b) at $x = 2.11$. (a), (b) Dark-bright rogue waves with single (dashed line for $d = 0$) and triple (solid line for $d = 3\pi/4$) compression points. The other parameters are the same as depicted in Fig. 1.

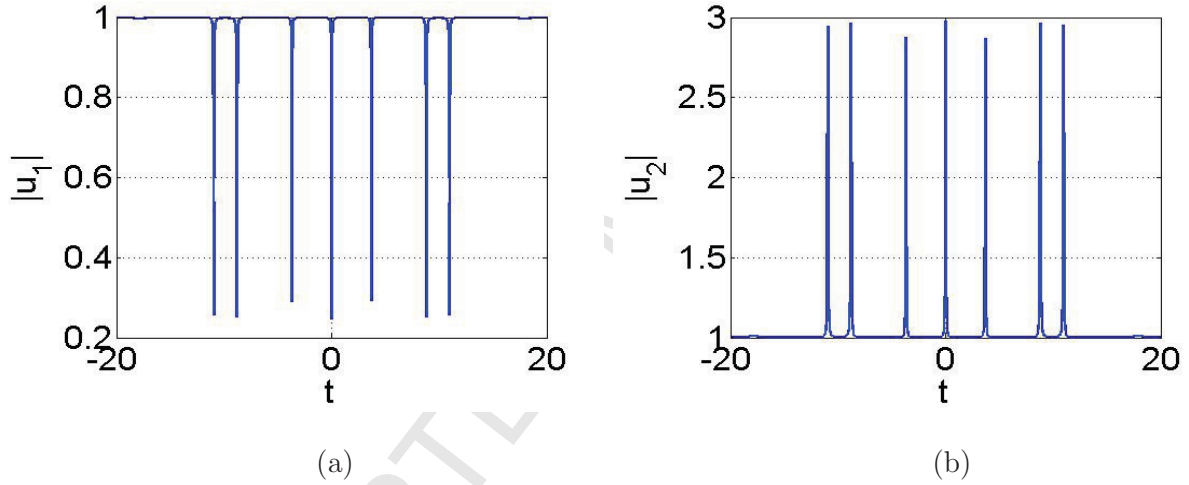


Fig. 3: (a), (b) Shape of dark-bright combs in u_1 and u_2 component with $d = 15\pi/4$ at $x = 2.11$. The other parameters are the same as depicted in Fig. 1.

Meanwhile, the propagation of rogue waves on periodic background can be shown by controlling the values of the constants \tilde{d} and \tilde{k} . For the choice of specific parameters the intensity profiles of the dark-bright rogue waves with triple compression points under the sinusoidal wave background are exhibited in Fig. 4. The constants \tilde{d} and \tilde{k} control the amplitude and period of the background wave, respectively.

To proceed, by returning to Eqs. (22a)-(22b) with $N = 2$, one can compute the explicit second-order rogue wave solution. Here we refrain from writing down the cumbersome expression of the higher-order solution, and merely focus on demonstrating the complex dynamics of it. At this time, the second-order rogue waves can be classified into two types, that is, the fundamental pattern and the triangular pattern (i.e. the celebrated “three sisters” rogue wave) [11]. As before, in the light of the formula (30), by varying the amplitude of the GVD-TOD periodic modulation, the higher-order rogue waves with multiple compression points can emerge. We show that in Fig. 5(a), one dark rogue wave split into two extra peaks in the temporal direction at $t = 0$ along with two normal dark

rogue waves distribute with a triangle in u_1 component. Also, for the bright case in u_2 component, the analogous wave phenomenon occurs as is seen in Fig. 5(b).

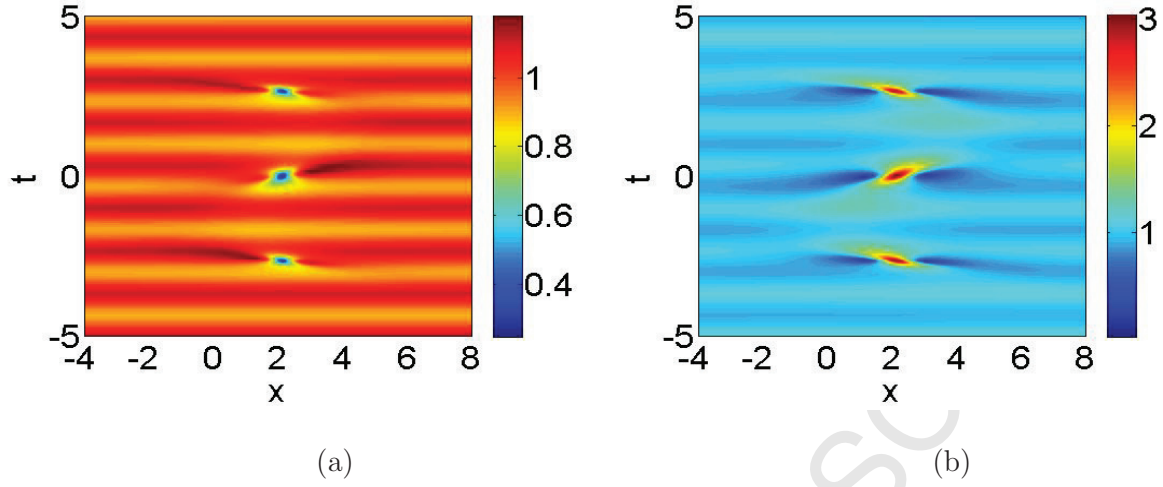


Fig. 4: Intensity of the solution (26a)-(26b) with $d = 3\pi/4, k = \pi/4, \tilde{d} = -0.1, \tilde{k} = 3\pi/2, A_0 = -2.10$ and $\nu = 0.1$. (a), (b) Dark-bright rogue waves with triple compression points under a sinusoidal wave background in u_1 and u_2 components.

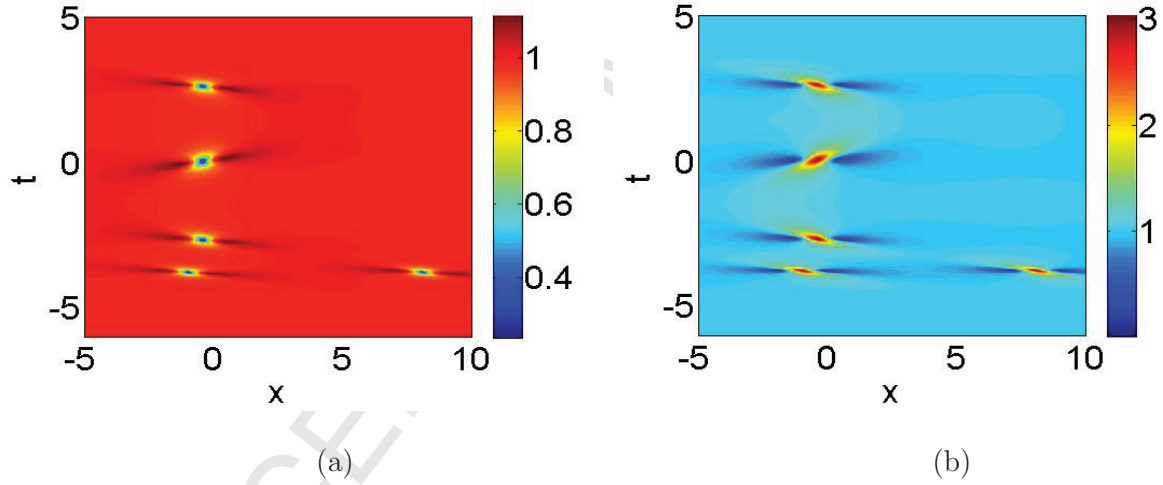


Fig. 5: Intensity of the second-order rogue wave solution given by Eqs. (22a)-(22b) with $N = 2, d = 3\pi/4, k = \pi/4, \tilde{d} = 0, m_0 = 5, m_1 = 0, n_0 = 1, n_1 = 0, A_0 = 0$ and $\nu = 0.1$. (a), (b) Dark-bright three sisters involving one rogue wave with triple compression points in u_1 and u_2 components.

5.2. Composite rogue waves

By means of the formulas (25a)-(25b) with $N = 1$, we can develop the rogue wave solution taking the form

$$u_1[1] = \sqrt{\frac{\alpha(t)}{\delta(t)}} e^{i\theta_1} \frac{(\tilde{G}_1 + i\tilde{H}_1)}{\tilde{F}}, \quad (31a)$$

$$u_2[1] = \sqrt{\frac{\alpha(t)}{\delta(t)}} e^{i\theta_2} \frac{(\tilde{G}_2 + i\tilde{H}_2)}{\tilde{F}}, \quad (31b)$$

where the corresponding polynomials are presented in appendix, and here we have taken $\beta(t) = \nu\alpha(t)$ with ν being a small real constant, and $m_0 = 10$, $n_0 = 0$ and $s_0 = 1/10$. At this time, it is particular to point out that the above solution is characterized by fourth degree polynomials. Consequently, there would appear composite states performing as rogue wave doublets (or rather pairs) when plotting the intensity profiles of the rogue waves described by Eqs. (31a)-(31b).

At this stage, as is mentioned in the above subsection, we identically select the periodic modulation functions taking the forms of Eqs. (27)-(28). Further, through the simple numerical calculations, we can infer that the maximum values of the wave amplitude in u_1 component arrive at $(x, A(t)) = (14.13, 0)$, $(x, A(t)) = (-14.12, -0.08)$, and in u_2 component, the corresponding position coordinates are $(x, A(t)) = (14.13, 0)$, $(x, A(t)) = (-14.00, 0.08)$. In analogous to the dark-bright case, here we assume the integration constant be $A_0 = 0$. Thus, with the help of the formula (30), on can show the rogue wave doublets with multiple compression points.

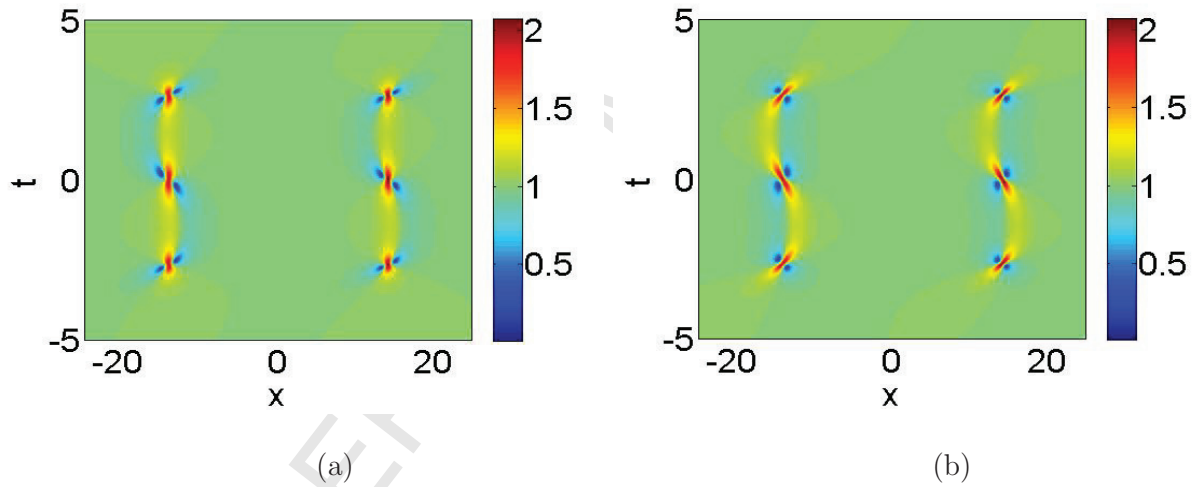


Fig. 6: Intensity of the solution (31a)-(31b) with $d = 3\pi/4$, $k = \pi/4$, $\tilde{d} = 0$, $A_0 = 0$ and $\nu = 0.1$. (a), (b) Rogue wave doublets with triple compression points in u_1 and u_2 components.

As is depicted in Fig. 6, we observe that two rogue waves involving triple compression points emerge on the temporal-spatial distribution plane in u_1 and u_2 components, respectively, which is fairly different from the ordinary composite rogue waves in the coupled constant-coefficient system. Meanwhile, in the similar way, by sufficiently enlarging the value of the amplitude of periodic modulation, the comb-like rogue wave doublets with sevenfold compression points can be produced, see Fig. 7. Here it is noteworthy that we only exhibit the shape of the comb-like structure at $x = 14.13$, while for $x = -14.12$ or $x = -14.00$, the situation is homologous yet the maximum values of the comb-like wave amplitudes are slightly less than that of the actual sates, and we neglect this kind of difference in the present paper.

Besides, as is discussed before, the rogue wave doublets with multiple compression points under periodic background can also be presented, see Fig. 8. The constants \tilde{d} and \tilde{k} play an identical part

in influencing the SPM-XPM periodic modulation.

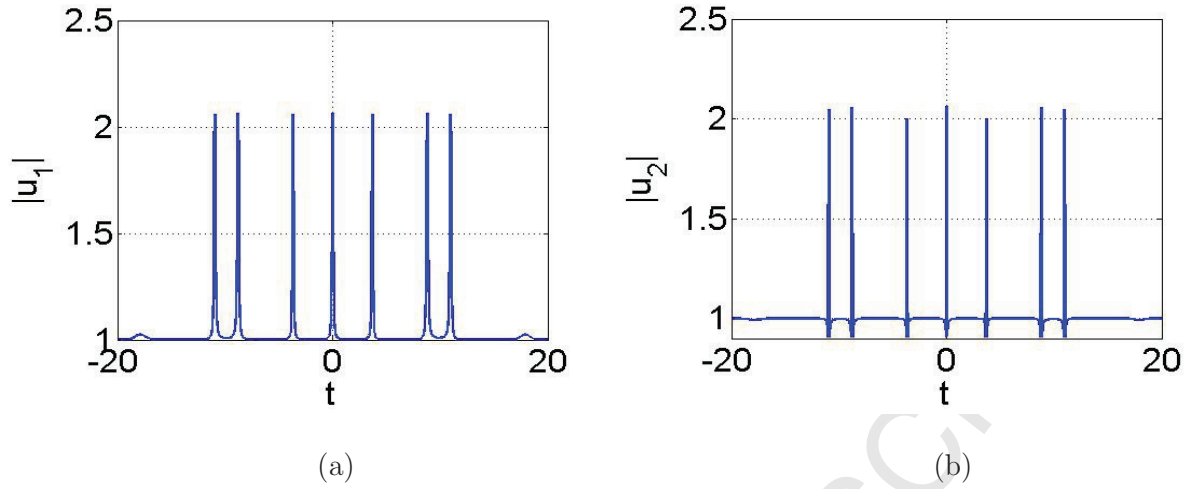


Fig. 7: (a), (b) Shape of comb doublets in u_1 and u_2 component with $d = 15\pi/4$ at $x = 14.13$. The other parameters are the same as depicted in Fig. 6.

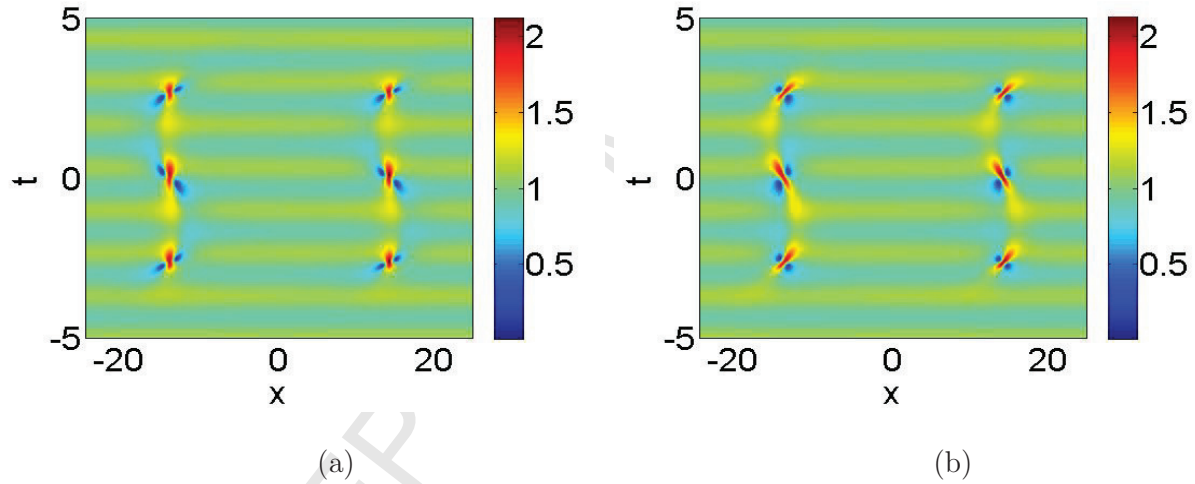


Fig. 8: Intensity of the solution (31a)-(31b) with $d = 3\pi/4$, $k = \pi/4$, $\tilde{d} = -0.1$, $\tilde{k} = 3\pi/2$, $A_0 = 0$ and $\nu = 0.1$. (a), (b) Rogue wave doublets with triple compression points under a sinusoidal wave background in u_1 and u_2 components.

Uteriorly, one can carry out the second-order rogue wave solution by means of Eqs. (25a)-(25b) with $N = 2$. In this status, the solution is constituted by the ratio of eighth or twelfth-order polynomials. As a consequence, the higher-order rogue waves are composite of four or six fundamental rogue waves and would exhibit more abundant patterns. Naturally, for the variable-coefficient case, the corresponding rogue wave quartets or sextets involving one or more rogue waves with multiple compression points (namely, the rogue wave cluster) can arise by adjusting the values of the periodic modulation coefficients. As an example, it is vividly displayed that in Fig. 9, two rogue waves in the direction of $t = 0$ separate into three compression points, together with two normal rogue waves appear with a quadrilateral in u_1 and u_2 components, respectively. In Fig. 10, we see that the rogue wave cluster including six rogue waves with triple compression points are shown. It is notable to remark that although the nonautonomous rogue wave quartets or sextets depicted in Figs. 9-10 in

u_1 and u_2 components are similar, yet the concrete maximum wave amplitudes and their coordinate positions are not identical in each component.

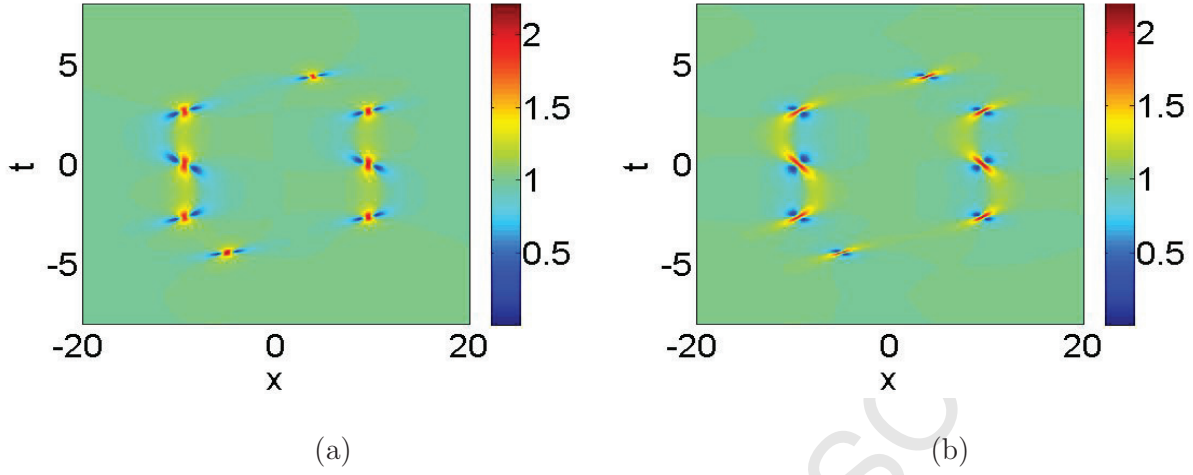


Fig. 9: Intensity of the second-order rogue wave solution given by Eqs. (25a)-(25b) with $N = 2, d = 3\pi/4, k = \pi/4, \tilde{d} = 0, m_0 = 0, m_1 = 1000, n_0 = 1, n_1 = 0, s_0 = 0, s_1 = 0, A_0 = 0$ and $\nu = 0.1$. (a), (b) Rogue wave quartets involving two rogue waves with triple compression points in u_1 and u_2 components.

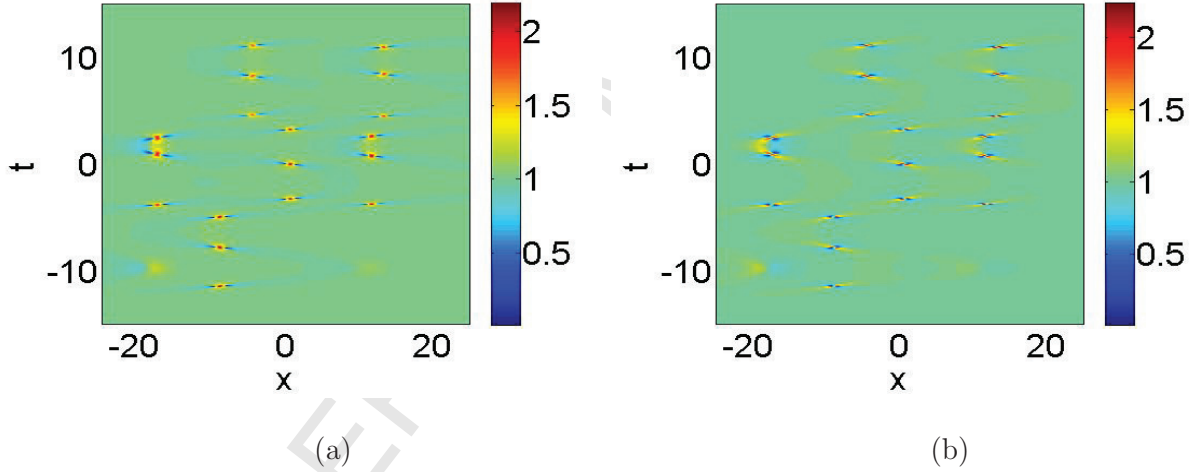


Fig. 10: Intensity of the second-order rogue wave solution given by Eqs. (25a)-(25b) with $N = 2, d = 5.8, k = \pi/4, \tilde{d} = 0, m_0 = 0, m_1 = 1000, n_0 = 0, n_1 = 0, s_0 = 0.1, s_1 = 0, A_0 = 0$ and $\nu = 0.1$. (a), (b) Rogue wave cluster involving six rogue waves with triple compression points in u_1 and u_2 components.

In the last of this section, we should mention that, the rogue wave solutions given in this paper can be reduced to the Manakov system by taking $\nu \rightarrow 0$ and $\delta(t)/\alpha(t)$ tend to a constant. On account of the presence of the higher-order effects, one can find that under identical parameter conditions compared to the Manakov system [22, 24, 27, 28], the ‘ridge’ [16, 31] of the rogue waves in Eqs. (1)-(2) is tilted to a certain extent, and the distributions of the rogue waves in the t dimension is contracted significantly, see the intensity profiles shown before.

6. Further properties of the dark rogue wave solution

At last, let us simply discuss some wave characteristics of the interesting dark rogue wave with multiple compression points. The difference between light intensity and CW background of the

nonautonomous dark rogue wave solution (26a) is defined as

$$\Delta I_c(x, t) = |u_1[1]|^2 - |u_{10}[1]|^2, \quad (32)$$

where $u_{10}[1] = \lim_{x \rightarrow \infty} u_1[1]$. Hereby, we can check

$$\int_{-\infty}^{+\infty} \Delta I_c(x, t) dx = 0,$$

which implies that for the dark rogue wave, the energy of the pump is preserved in the fiber with periodic modulation characteristics. However, it is clearly seen that in Fig. 11(a) the light intensity of the nonautonomous dark rogue wave solution is always lower than its CW background, which is different from the corresponding situation of bright case reported in [41].

Next, we can obtain the energy pulse of the nonautonomous dark rogue wave defined by

$$E_p(t) = \int_{-\infty}^{\infty} |u_1[1] - u_{10}[1]|^2 dx. \quad (33)$$

We show that the relative energy pulse is coincide well with the compression points, and with the amplitude of the periodic modulation increasing, the number of maximum points of the energy pulse also increases, see Fig. 11(b).

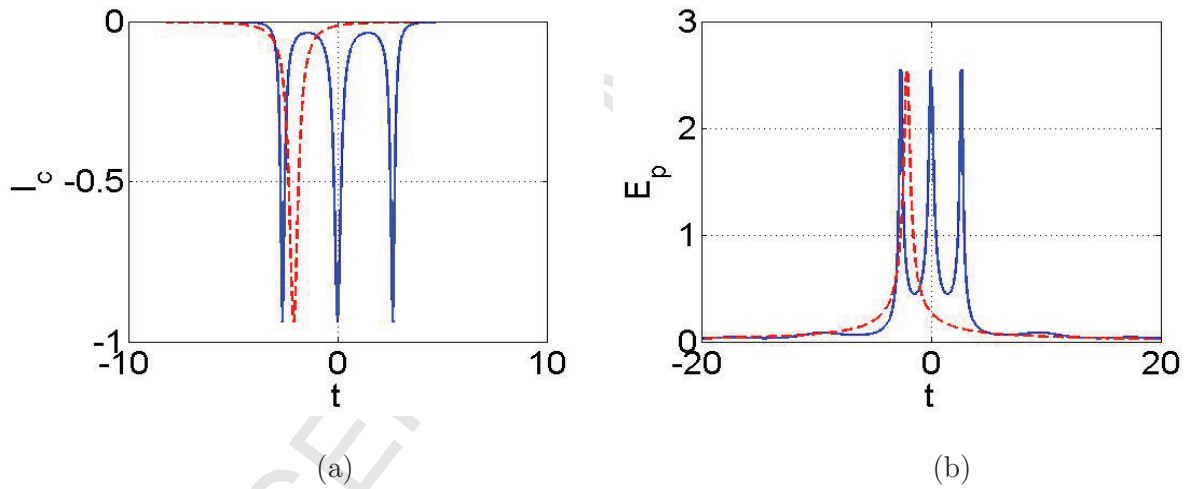


Fig. 11: (a) Shape of the difference between light intensities and CW background of the solution (26a) at $x = 2.11$ with $d = 0$ (dashed line) and $d = 3\pi/4$ (solid line); (b) Shape of the energy pulse given by (33) with $d = 0$ (dashed line) and $d = 3\pi/4$ (solid line). The other parameters are the same as depicted in Fig. 2.

7. Conclusion

In summary, we presented two types of N th-order rogue wave solutions under different relative frequencies for the VCCH equations. An exact calculation formula depending on the amplitude of the periodic modulation for the number of the compression points of the rogue waves was given. Thus, the dark-bright and composite rogue waves with multiple compression points, and even the corresponding comb-like structures were generated by choosing sufficiently large periodic modulation amplitudes in the coefficients of the VCCH equations. Moreover, for higher-order case, the dark-bright three sisters involving one rogue wave with triple compression points, the rogue wave quartets

involving two rogue waves with triple compression points, and the rogue wave cluster involving six rogue waves with triple compression points were visually shown by selecting the adequate modulation coefficients. Further, some wave characteristics of the dark rogue wave solution were discussed in the last of the paper. Our work generalizes Tiofack' very recent results into the vector case, and it is expected that these findings may provide some theoretical assistance to the experimental control and manipulation of vector rogue wave dynamics in inhomogeneous fiber systems, etc.

Acknowledgment

One of the authors X. Wang would like to thank Professor Y. Chen, Doctor L.M. Ling and L.C. Zhao for their valuable suggestions and discussions.

Appendix:Polynomials

$$\begin{aligned}
 G_1 &= [12x^2 + (4\sqrt{3}z_1 + 4z_1)x + (756\nu^2 - 72\nu z_1 + 24\sqrt{3}\nu z_1 + 48\sqrt{3})A(t)^2 + ((8\sqrt{3}z_1 \\
 &\quad - 144\nu + 24z_1)x + 360\sqrt{3}\nu - 24\sqrt{3}\nu z_1 - 24\nu z_1 + 40\sqrt{3}z_1 + 120z_1 + 24)A(t) + 297 \\
 &\quad + \sqrt{3} + \sqrt{3}z_1 + 3z_1], \\
 H_1 &= [(6 + 2\sqrt{3}z_1)x + (8\sqrt{3}z_1 - 36\nu z_1 - 12\sqrt{3} + 18\nu + 12z_1 - 30\sqrt{3}\nu z_1)A(t) \\
 &\quad + (33\sqrt{3} - 29z_1 - 3 - 19\sqrt{3}z_1)], \\
 G_2 &= [12x^2 + (4\sqrt{3}z_1 + 4z_1)x + (756\nu^2 - 72\nu z_1 + 24\sqrt{3}\nu z_1 + 48\sqrt{3})A(t)^2 + ((8\sqrt{3}z_1 \\
 &\quad + 24z_1 - 144\nu)x + 360\nu\sqrt{3} - 24\sqrt{3}\nu z_1 - 24\nu z_1 + 40\sqrt{3}z_1 + 120z_1 + 24)A(t) + 297 \\
 &\quad + \sqrt{3} - \sqrt{3}z_1 - 3z_1], \\
 H_2 &= [(-6 + 2\sqrt{3}z_1)x - (30\sqrt{3}\nu z_1 + 36\nu z_1 + 12\sqrt{3} + 8\sqrt{3}z_1 + 12z_1 + 18\nu)A(t) \\
 &\quad - (21\sqrt{3}z_1 + 31z_1 + 27\sqrt{3} + 3)], \\
 F &= 2[3x^2 + (z_1 + \sqrt{3}z_1)x + (189\nu^2 - 18\nu z_1 + 12\sqrt{3} + 6\sqrt{3}\nu z_1)A(t)^2 + ((6z_1 - 36\nu + 2\sqrt{3}z_1)x \\
 &\quad + 10\sqrt{3}z_1 + 30z_1 + 90\sqrt{3}\nu - 6\nu z_1 + 6 - 6\sqrt{3}\nu z_1)A(t) + 75 + \sqrt{3}], \\
 \rho_1 &= \frac{(3 + \sqrt{3}z_1 + 2z_1)}{(6 + 6i + \sqrt{3}z_1 + z_1 + 3iz_1 + \sqrt{3}iz_1)}, \quad \rho_2 = \frac{(-3 + \sqrt{3}z_1 + 2z_1)}{(-6 - 6i + \sqrt{3}z_1 + z_1 + 3iz_1 + \sqrt{3}iz_1)}, \\
 \tilde{G}_1 &= 2304x^4 + 4608\sqrt{3}x^3 - 932352x^2 - 920576\sqrt{3}x + 81(363\nu^2 + 16)^2A(t)^4 + (-14256\nu(363\nu^2 \\
 &\quad + 16)x - 216\sqrt{3}(192 + 16335\nu^3 + 4356\nu^2 + 1040\nu))A(t)^3 + ((940896\nu^2 + 13824)x^2 \\
 &\quad + 288\sqrt{3}(4059\nu^2 + 112 + 792\nu)x - 124416\nu - 63053856\nu^2 + 2797056)A(t)^2 + (-76032\nu x^3 \\
 &\quad - 3456\sqrt{3}(37\nu + 4)x^2 + 15342336\nu x + 768\sqrt{3}(-3576 + 13507\nu))A(t) + 93077504,
 \end{aligned}$$

$$\begin{aligned}
 \tilde{H}_1 &= -2304\sqrt{3}x^4 + 4608x^3 + 923136\sqrt{3}x^2 - 930816x - 81\sqrt{3}(363\nu^2 + 16)^2 A(t)^4 \\
 &\quad + (14256\sqrt{3}\nu(363\nu^2 + 16)x + 235224\nu^3 - 41472 - 940896\nu^2 + 217728\nu)A(t)^3 \\
 &\quad + (-864\sqrt{3}(1089\nu^2 + 16)x^2 + (228096\nu + 256608\nu^2 - 41472)x + 288\sqrt{3}(-9488 + 384\nu \\
 &\quad + 218343\nu^2))A(t)^2 + (76032\sqrt{3}\nu x^3 - (72576\nu + 13824)x^2 - 2304\sqrt{3}(8 + 6617\nu)x \\
 &\quad - 2783232 - 573696\nu)A(t) - 91238400\sqrt{3}, \\
 \tilde{G}_2 &= 2304x^4 + 4608\sqrt{3}x^3 - 932352x^2 - 920576\sqrt{3}x + 81(363\nu^2 + 16)^2 A(t)^4 + (-14256\nu(363\nu^2 \\
 &\quad + 16)x - 216\sqrt{3}(-192 - 4356\nu^2 + 1040\nu + 16335\nu^3))A(t)^3 + ((940896\nu^2 + 13824)x^2 \\
 &\quad + 288\sqrt{3}(112 + 4059\nu^2 - 792\nu)x + 124416\nu - 63053856\nu^2 + 2797056)A(t)^2 + (-76032\nu x^3 \\
 &\quad - 3456\sqrt{3}(37\nu - 4)x^2 + 15342336\nu x + 768\sqrt{3}(13507\nu + 3576))A(t) + 93077504, \\
 \tilde{H}_2 &= 2304\sqrt{3}x^4 - 4608x^3 - 923136\sqrt{3}x^2 + 930816x + 81\sqrt{3}(363\nu^2 + 16)^2 A(t)^4 \\
 &\quad + (-14256\sqrt{3}\nu(363\nu^2 + 16)x - 235224\nu^3 - 41472 - 940896\nu^2 - 217728\nu)A(t)^3 \\
 &\quad + (864\sqrt{3}(1089\nu^2 + 16)x^2 + (228096\nu - 256608\nu^2 + 41472)x - 288\sqrt{3}(-9488 - 384\nu \\
 &\quad + 218343\nu^2))A(t)^2 + (-76032\sqrt{3}\nu x^3 + (72576\nu - 13824)x^2 + 2304\sqrt{3}(-8 + 6617\nu)x \\
 &\quad - 2783232 + 573696\nu)A(t) + 91238400\sqrt{3}, \\
 \tilde{F} &= -4608x^4 + 1837056x^2 + 4096\sqrt{3}x - 162(363\nu^2 + 16)^2 A(t)^4 + (28512\nu(363\nu^2 + 16)x \\
 &\quad + 1728\sqrt{3}\nu(128 + 1089\nu^2))A(t)^3 + ((-1881792\nu^2 - 27648)x^2 - 4608\sqrt{3}(99\nu^2 + 8)x \\
 &\quad + 124910208\nu^2 - 5566464)A(t)^2 + (152064\nu x^3 + 27648\sqrt{3}\nu x^2 - 30311424\nu x \\
 &\quad - 5563392\sqrt{3}\nu)A(t) - 184324096.
 \end{aligned}$$

References

- [1] C. Kharif, E. Pelinovsky, Eur. J. Mech. B Fluids 22 (2003) 603.
- [2] K. Dysthe, H.E Krogstad, P. Müller, Annu. Rev. Fluid Mech. 40 (2008) 287.
- [3] D.R. Solli, C. Ropers, P. Koonath, B. Jalali, Nature 450 (2007) 1054.
- [4] Y.V. Bludov, V.V. Konotop, N. Akhmediev, Phys. Rev. A 80 (2009) 033610.
- [5] L. Stenflo, M. Marklund, J. Plasma Phys. 76 (2010) 293.
- [6] W.M. Moslem, P.K. Shukla, B. Eliasson, Eur. Phys. Lett. 96 (2011) 25002.
- [7] Z.Y. Yan, Commun. Theor. Phys. 54 (2010) 947.
- [8] N. Akhmediev, A. Ankiewicz, M. Taki, Phys. Lett. A 373 (2009) 675.
- [9] V. E. Zakharov, A. A. Gelash, Phys. Rev. Lett. 111 (2013) 054101.
- [10] D.H. Peregrine, J. Austral. Math. Soc. B: Appl. Math. 25 (1983) 16.
- [11] A. Ankiewicz, D.J. Kedziora, N. Akhmediev, Phys. Lett. A 375 (2011) 2782.
- [12] D.J. Kedziora, A. Ankiewicz, N. Akhmediev, Phys. Rev. E 84 (2011) 056611.
- [13] D.J. Kedziora, A. Ankiewicz, N. Akhmediev, Phys. Rev. E 88 (2013) 013207.
- [14] A. Chabchoub, N.P. Hoffmann, N. Akhmediev, Phys. Rev. Lett. 106 (2011) 204502.
- [15] A. Chabchoub, N. Hoffmann, M. Onorato, Slunyaev, et al., Phys. Rev. E 86 (2012) 056601.
- [16] A. Ankiewicz, J.M. Soto-Crespo, N. Akhmediev, Phys. Rev. E 81 (2010) 046602.
- [17] L.H. Wang, K. Porsezian, J.S. He, Phys. Rev. E 87 (2013) 053202.
- [18] A. Ankiewicz, Y. Wang, S. Wabnitz, N. Akhmediev, Phys. Rev. E 89 (2014) 012907.
- [19] X. Wang, B. Yang, Y. Chen, Y.Q. Yang, Phys. Scr. 89 (2014) 095210.
- [20] F. Baronio, A. Degasperis, M. Conforti, S. Wabnitz, Phys. Rev. Lett. 109 (2012) 044102.
- [21] F. Baronio, M. Conforti, A. Degasperis, S. Lombardo, M. Onorato, S. Wabnitz, Phys. Rev. Lett. 113 (2014) 034101.

- [22] L.C. Zhao, J. Liu, J. Opt. Soc. Am. B 29 (2012) 3119.
- [23] L.C. Zhao, G.G. Xin, Z.Y. Yang, Phys. Rev. E 90 (2014) 022918.
- [24] L.M. Ling, B.L. Guo, L.C. Zhao, Phys. Rev. E 89 (2014) 041201.
- [25] L. Wang et al., Commun. Nonlinear Sci. Numer. Simul. 40 (2016) 216.
- [26] W.R. Sun, B. Tian, R.X. Liu, D.Y. Liu, J. Math. Anal. Appl. 424 (2015) 1006.
- [27] S.H. Chen, L.Y. Song, Phys. Rev. E 87 (2013) 032910.
- [28] S.H. Chen, Phys. Lett. A 378 (2014) 2851.
- [29] X. Wang, Y.Q. Li, Y. Chen, Wave Motion 51 (2014) 1149.
- [30] F. Baronio, M. Conforti, A. Degasperis, S. Lombardo, Phys. Rev. Lett. 111 (2013) 114101.
- [31] L.J. Li, Z.W. Wu, L.H. Wang, J.S. He, Ann. Phys. 334 (2013) 198.
- [32] A. Chowdury, D.J. Kedziora, A. Ankiewicz, N. Akhmediev, Phys. Rev. E 91 (2015) 032928.
- [33] C. Liu, Z.Y. Yang, L.C. Zhao, W.L. Yang, Phys. Rev. E 91 (2015) 022904.
- [34] C. Liu, Z.Y. Yang, L.C. Zhao, W.L. Yang, Ann. Phys. 362 (2015) 130.
- [35] L.C. Zhao, J. Liu, Phys. Rev. E 87 (2013) 013201.
- [36] S. Loomba, H. Kaur, R. Gupta, C.N. Kumar, et al., Phys. Rev. E 89 (2014) 052915.
- [37] Z.Y. Yan, C.Q. Dai, J. Opt. 15 (2013) 064012.
- [38] S. Loomba, R. Pal, C.N. Kumar, Phys. Rev. E 92 (2015) 033811.
- [39] W.P. Zhong, M. Belić, B.A. Malomed, Phys. Rev. E 92 (2015) 053201.
- [40] L. Wang, X. Li, F.H. Qi, L.L. Zhang, Ann. Phys. 359 (2015) 97.
- [41] C.G.L. Tiofack, S. Coulibaly, M. Taki, Phys. Rev. A 92 (2015) 043837.
- [42] R.S. Tasgal, M. J. Potasek, J. Math. Phys. 33 (1992) 1208.
- [43] J.S. He, Y.S. Tao, K. Porsezian, A.S. Fokas, J. Nonlinear Math. Phys. 20 (2013) 407.
- [44] M.J. Ablowitz, H. Segur, Solitons and the inverse scattering transform, Philadelphia: Siam, 1981.
- [45] F. Baronio, S. Chen, P. Grelu, S. Wabnitz, M. Conforti, Phys. Rev. A 91 (2015) 033804.
- [46] L.C. Zhao, L. M. Ling, J. Opt. Soc. Am. B 33 (2016) 850.
- [47] B.L. Guo, L.M. Ling, Q.P. Liu, Phys. Rev. E 85 (2012) 026607.
- [48] B.L. Guo, L.M. Ling, Q.P. Liu, Stud. Appl. Math. 130 (2013) 317.
- [49] Zhaqilao, Phys. Lett. A 377 (2013) 855.
- [50] N.V. Priya, M. Senthilvelan, Commun. Nonlinear Sci. Numer. Simul. 20 (2015) 401.
- [51] X. Wang, Y.Q. Li, F. Huang, Y. Chen, Commun. Nonlinear Sci. Numer. Simul. 20 (2015) 434.
- [52] C.H. Gu, H.S. Hu, Z.X. Zhou, Darboux transformations in integrable systems: theory and their applications to geometry, Springer-Verlag, New York, 2005.